NASA TECHNICAL NOTE

NASA TN D-8241

NASA TN D-8241

COSMOGENIC RADIONUCLIDES IN STONE METEORITES

Philip J. Cressy, Jr.

Goddard Space Flight Center

Greenbelt, Md. 20771

NATIONAL AERONAUTICS AND SPACE ADMINISTRATION • WASHINGTON, D. C. • MAY 1976

1. Report No.	2. Government Accession No.	3 Recipient's Catalog No
NASA TN D-8241		

4. Title and Subtitle	5. Report Date
Cosmogenic Radionuclides in Stone Meteorites	May 1976
	6. Performing Organization Code 923
7. Author(s) Philip J. Cressy, Jr.	8 Performing Organization Report No. G-7658
9. Performing Organization Name and Address Goddard Space Flight Center Greenbelt, Maryland 20771	10 Work Unit No. 195-22-04-03
	11. Contract or Grant No.
	13. Type of Report and Period Covered Technical Note
12. Sponsoring Agency Name and Address National Aeronautics and Space Administration Washington, D.C. 20546	14 Sponsoring Agency Code

15. Supplementary Notes

16. Abstract

This document presents the techniques and compilation of results of cosmogenic ^{26}Al measurements at Goddard Space Flight Center on 91 samples of 76 stone meteorites. Short-lived radionuclides, including ^{22}Na, ^{46}Sc, ^{54}Mn, and ^{60}Co, were measured in 13 of these meteorites. About one-third of these data has not previously been published. The results are discussed briefly in terms of (1) depletion of ^{26}Al and natural potassium due to weathering, (2) possible exposure of several chondrites to an unusually high cosmic-ray flux, (3) comparison of ^{26}Al, ^{22}Na, ^{46}Sc, and ^{54}Mn in chondrites with the spallation $^{22}Ne/^{21}Ne$ ratio as a shielding indicator, and (4) comparison of ^{26}Al - $^{22}Ne/^{21}Ne$ data for achondrite classes with the chondrite trend.

17. Key Words (Selected by Author(s))	18 Distribution Statement
Meteorites, Chondrites, Achondrites, Radioactivity, ^{26}Al, Cosmic-ray shielding, ^{22}Na, ^{46}Sc, ^{54}Mn, ^{60}Co, K	Unclassified–Unlimited Cat. 89

19. Security Classif. (of this report)	20 Security Classif. (of this page)	21. No. of Pages	22 Price*
Unclassified	Unclassified	28	$3.75

For sale by the National Technical Information Service, Springfield, Virginia 22161

Page intentionally left blank

Page intentionally left blank

CONTENTS

COSMOGENIC RADIONUCLIDES IN STONE METEORITES

Philip J. Cressy, Jr.
Goddard Space Flight Center

INTRODUCTION

The purpose of this document is to present a compilation of the results of a decade of measurements of cosmic-ray-induced radioactivity in stone meteorites. Part of the data has appeared in the published literature (References 1 through 8) and is included for completeness, but is not extensively discussed.* Results of incomplete projects are included here in the hope that investigators actively engaged in meteorite research will find the information of value.

The short- and long-lived radionuclide contents of a meteorite specimen depend on the chemical composition of the sample, on the depth from the preatmospheric surface of the meteorite, on the preatmospheric size of the meteorite, its terrestrial and cosmic-ray exposure ages, and the cosmic-ray flux to which the meteorite was exposed in space. The knowledge of nuclear production systematics in meteorites has grown in recent years in the areas of target element production rates (References 2 and 9) and depth effects (References 6 and 8). The interpretation of radionuclide measurements is beginning to fulfill its potential as a tool in understanding the cosmic-ray environment and the origins of meteorites.

---

*Cressy, P.J., "^{26}Al in Kenna and Other Ureilites," *Geochim. Cosmochim. Acta*, 1976, in press.

Cressy, P.J. and D. D. Bogard, "On the Calculation of Cosmic-ray Exposure Ages of Stone Meteorites," *Geochim. Cosmochim. Acta*, 1976, in press.

Herzog, G. F. and P. J. Cressy, "Diogenite Exposure Ages," *Geochim. Cosmochim. Acta*, 1976, in press.

Herzog, G. F. and P. J. Cressy, "The Cosmic-ray Exposure of Aubrites," 1976, in preparation

Fudali, R. F. and P. J. Cressy, "Investigation of a New Stony Meteorite from Mauritania with Some Additional Data on Its find Site: Aouelloul Crater," *Earth and Planetary Science Letters*, 1976, in press

Herzog, G. F. and P. J. Cressy, "^{26}Al Losses from Weathered Chondrites," *Meteoritics*, 1976, in press.

MEASUREMENT SYSTEM

Whole rock and powdered meteorite specimens were measured for gamma-ray emitting radionuclides in a nondestructive, dual parameter, gamma coincidence counting system. The essential components of the detection system are:

- A clean steel shield, 137-cm outside length, 81-cm outside width and height, 15-cm wall thickness, with a 5-cm thickness of lead bricks on top;
- A plastic scintillator anticoincidence detector, 51 cm long, 41-cm outside diameter, and 18-cm inside diameter, with six RCA 8054 photomultiplier tubes at 60° spacings on one end;
- A 5-cm thickness of borated paraffin on top of the anticoincidence detector (inside the shield); and
- Two low background 10- by 10-cm (4- by 4-in.) NaI(TI) detectors, mounted in lucite tubes for geometric reproducibility, and each including
  - 7.6-cm unactivated NaI light pipe,
  - OFHC copper shell,
  - RCA 4521 phototube,
  - <1 ppm K contamination, and
  - 8 percent resolution for ^{137}Cs gamma-ray (0.661 MeV).

Anticoincidence gating is achieved by summing outputs from opposed phototubes and routing the resulting three signals through separate amplifiers and baseline restorers into single channel analyzers. The analyzer windows are set so that upper level discriminator outputs correspond to cosmic-ray events ($E > 3$ MeV, up to hundreds of MeV), while the windows correspond primarily to natural and to Compton-scattered events ($0.05 < E < 3$ MeV). These two sets of outputs are routed respectively to two coincidence modules which are set to deliver gating outputs when any two inputs are in time coincidence (~ 1 μs). The outputs are applied to the anticoincidence inputs to the pulse height analyzer.

Sample pulses are amplified, passed through digital gain/zero stabilizers, and entered into a 4096-channel dual parameter pulse height analyzer. The analyzer stores pulses as coincident or noncoincident events, with a resolving time of ~ 1 μs. The customary counting matrix is 64 by 64 channels, encompassing 0.1 to 3 MeV from each detector. The 64-channel conversion provides only adequate effective resolution for noncoincident events, but is excellent for coincident events; the latter are of primary importance to these studies.

SAMPLE AND BACKGROUND COUNTING

Whole or powdered meteorite samples were placed in lucite sample holders (selected because of typically high radiochemical purity) for nondestructive counting. For whole samples,

lucite rings (approximately 1- or 6-mm thickness, and with 5-, 7.6-, 10.2-, or 12.7-cm inside diameter) were used with ~1-mm thick end plates. For powdered samples, lucite containers (2.5-, 5.1-, 7.6-, or 10.2-cm inside diameters and 0.6, 1.2, 1.9, or 2.5 cm deep) were used. The assembled sample holder was bolted (stainless steel threaded rods) to the end of one of the sodium iodide detector holders, ensuring that sample position could be duplicated with calibration standards.

BACKGROUNDS

Background measurements were made using 150-μm dunite or nickel powder (depending on sample density). Initially the background samples were counted in the same geometries as the meteorite specimens. For powdered specimens, a lucite container was filled with dunite powder to the sample's level. For whole specimens, a mock-up was made (and later used for calibration sources). The meteorite specimen was wrapped in aluminum foil. A second layer was carefully formed around the sample and coated with a surface-hardening epoxy resin. A seam was left so that the shell could later be opened and the sample removed. The empty shell was then sealed and further coated, leaving an opening at the top (in its counting position) through which nickel powder was introduced to the desired weight. Under these conditions the dunite and nickel powdered background samples had bulk and electronic densities closely approximating those of powdered and whole stone meteorite samples, respectively.

After many exact mock-up backgrounds were run, it became clear that background levels varied systematically with the separation distance of the two sample detectors and were apparently not influenced by sample shape or even, for the range of samples studied, sample mass. Accumulated background counting rates (B) for the energy regions of interest were correlated with detector spacing (S) by unweighted least squares regression analysis, yielding equations of the form:

$$B = a_0 + a_1 S + a_2 S^2$$

In no case was there statistical justification for a third order fit; in some cases the second order term was unjustified statistically. Standard deviations were calculated from the differences between observed and calculated background counting rates. These calculated uncertainties for the background equations were similar in magnitude to measured uncertainties in typical 7000- to 10000-min background runs. Backgrounds calculated by this means were considered more reliable than the measured backgrounds for any individual sample. The procedure of measuring a background for each sample was discontinued. Thereafter, dunite or nickel backgrounds were measured about once a month to cover the range of expected detector spacings, to improve the confidence level of the equations, and to ensure the continued validity of the equations over time.

Table 1 lists the radioactive species of interest in this work, the appropriate gamma-ray energies and coincidences, the calculated background equations (in counts per minute for S in centimeters), the R^2 goodness of fit of the equations to the input data, and the calculated standard deviations to be used with the equations. The summation symbol (Σ) indicates that data along two analyzer axes are summed; for example,

$$\sum X_{0.51}\, Y_{1.27} + X_{1.27}\, Y_{0.51\ MeV}$$

Energy ranges used in counting rate calculations varied from ±0.05 MeV at low energies to ±0.10 MeV for higher energies. In cases where R^2 ~0.7, the counting rates were so low and varied so little with S that statistical fluctuations in counting rate measurements were major factors in the R^2 calculations.

Table 1
Background Equations

Radioactivity	Energy, MeV	Background, cpm	±σ	R^2
^{22}Na, ^{26}Al	0.51 X 0.51	$0.0719 - 0.129S + 0.00101S^2$	0.0025	0.96
^{22}Na	Σ 0.51 X 1.27	$0.0489 - 0.0101S + 0.00086S^2$	0.0036	0.86
^{22}Na, ^{26}Al	Σ 0.51 X 1.80	$0.0839 - 0.0184S + 0.00160S^2$	0.0050	0.91
^{26}Al	Σ 0.51 X 2.32	$0.0179 - 0.0031S + 0.00025S^2$	0.0016	0.78
U	Σ 0.61 X 0.77	$0.0431 - 0.0094S + 0.00087S^2$	0.0031	0.85
U	Σ 0.61 X 1.12 to 1.24	$0.0452 - 0.0082S + 0.00058S^2$	0.0032	0.86
U	Σ 0.61 X 1.38 to 1.51	$0.0361 - 0.0081S + 0.00067S^2$	0.0025	0.87
Th	Σ 0.28 X 2.61	$0.0254 - 0.0021S$	0.0021	0.72
Th	Σ 0.58 X 2.61	$0.0281 - 0.0049S + 0.00031S^2$	0.0017	0.87
Th	Σ 0.86 X 2.61	$0.0113 - 0.0021S + 0.00014S^2$	0.0014	0.66
^{60}Co	Σ 1.17 X 1.33	$0.0111 - 0.0021S + 0.00019S^2$	0.0010	0.69
^{40}K	Σ 1.46	$2.158 + 0.0612S + 0.0136S^2$	0.053	0.95

Figure 1 shows the data and calculated correlation lines for the 0.51- X 0.51- and 0.51- X 2.32-MeV background counting rates versus detector spacing. The trend toward decreasing background with increasing detector spacing is common to all but one case listed in table 1. The singular exception is the ^{40}K background, shown in figure 2 for each detector and for the sum. It is clear that the increasing total background with spacing is due primarily to the background variation of one sample detector. The position in the shield of that detector (Y) varies with sample thickness, while the X detector is kept in a fixed position. The Y detector moves nearer to the end of the anticoincidence mantle as sample thickness, and

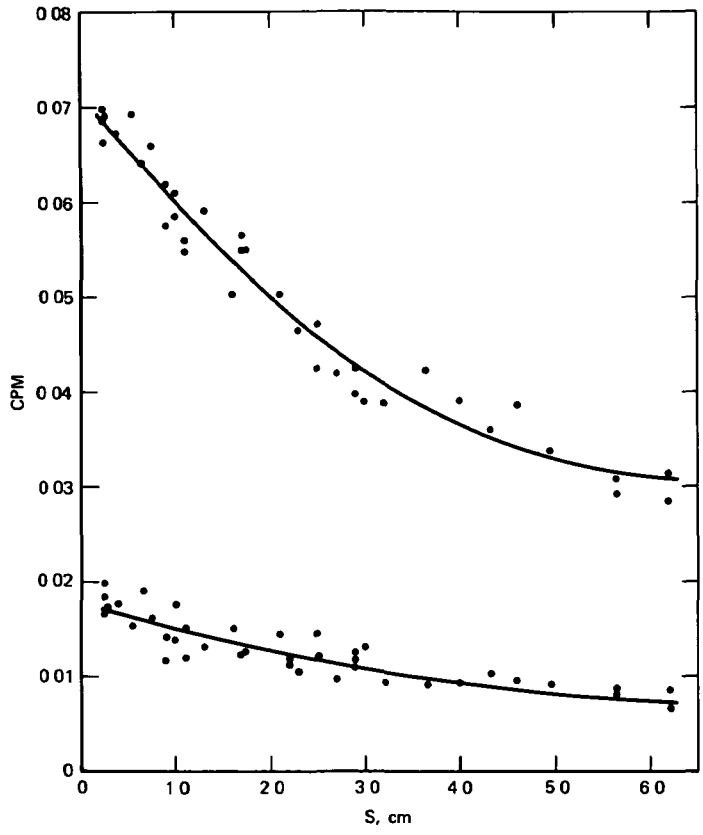

Figure 1. Coincidence background counting rates for 0.51- X 0.51- (top) and 0.51- X 2.32-MeV (bottom) plotted against detector spacing. The regression equations are given in table 1.

thus detector spacing, increases. Six conventional photomultiplier tubes, containing small but measurable amounts of K, U, and Th, are affixed to that end of the anticoincidence detector. Thus, as the Y detector is moved closer to these phototubes, the noncoincident background due to these naturally radioactive species increases.

CALIBRATION

Standardized sources of ^{22}Na, ^{26}Al, ^{40}K, ^{46}Sc, ^{54}Mn, ^{60}Co, U, and Th were used, as appropriate, to calibrate counting yields for individual meteorite sample geometries. All sources were obtained commercially (^{40}K as reagent-grade KCl) with listed calibration uncertainties of $\leq$5 percent. All calibrations were compared with certified standards used by Battelle Pacific Northwest Laboratories, resulting in revising the specific activities of the ^{26}Al, ^{46}Sc, and ^{54}Mn sources. The ^{26}Al source was corrected by quantitatively comparing coincident and single counting rates with a National Bureau of Standards ^{22}Na source (± 2 percent) in the same geometry. The revised ^{26}Al calibration was confirmed with the Battelle ^{26}Al standard.

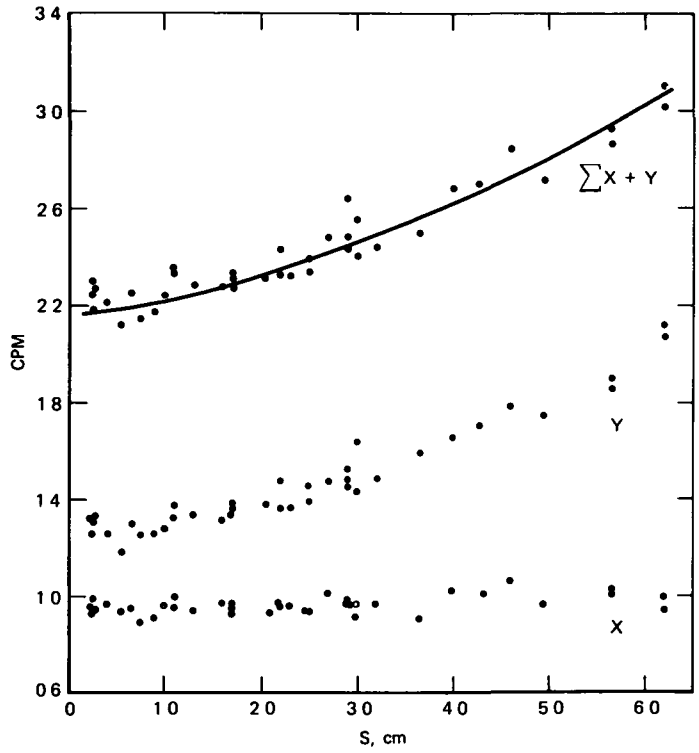

Figure 2. Net potassium background counting rates for the individual detectors and for their sum plotted against detector spacing. The equation for the sum of X and Y is given in table 1. The X distribution remains flat because the distance from that detector to the primary K source, the anticoincidence phototubes, remains constant (see text). The Y background, and thus the sum, increases with S because that detector is moved nearer the phototubes with increasing sample size.

Standards were mixed with 150-μm dunite or iron powders in order to simulate the densities of powdered or whole rock stone meteorite samples, respectively. The appropriate powder mixtures were placed directly in lucite holders, or into epoxy-coated mockups (discussed above), to duplicate sample geometries. In a few cases where samples were thin ($\leqslant$0.5 cm) slices of larger specimens, epoxy shells were not made. Instead, a thick layer of aluminum foil was shaped around the sample, filled with the proper mass of the standard of interest, and manually smoothed flat to fit the sample's holder.

Counting duplicate small samples demonstrated source uniformity at least down to the 10-g level. Repeated filling, mounting, and counting mockups or shaped foils yielded agreement between runs within counting statistics. All cosmogenic radionuclide measurements were calibrated by direct comparison with standards in identical geometries. This was generally true of ^{40}K, and less so for U and Th. In some cases in which the K, U, or Th contents were not required to high accuracy, counting yields were estimated from other samples of similar size/shape; uncertainties in calibration estimates were included in the calculations of element concentration.

Table 2 lists measured counting yields for a range of representative sample geometries. The samples are identified by mass and detector spacing. For coincident events, yields were obtained from the difference between standard and background counting rates, divided by the source specific activity (or mass in the cases of U and Th). For K, the source counting rate for the 1.46-MeV full energy peak was first corrected for the counting rate in adjacent nonpeak channels. A net background counting rate, obtained similarly (see table 1), was subtracted, and the difference divided by the mass of potassium in the source. For actual samples, this technique minimized potential interference due to scattering of higher energy gamma rays. Thus, for the specific channels used in this work:

$$\epsilon_K = \frac{R(\text{ch } 30\text{-}33) - R(28 + 29 + 34 + 35)}{M_K}$$

No calibrated source was available for ^{48}V (0.98 X 1.31 MeV). When this nuclide was detected in the coincidence spectrum of a recently-fallen chondrite, the counting yield was interpolated from those of ^{60}Co (1.17 X 1.33 MeV) and ^{46}Sc (0.89 X 1.12).

Table 2
Representative Counting Yields

Nuclide	Energy (MeV)	Sample Mass and Detector Spacing			
		203 g 4.9 cm	284 g 5.4 cm	50 g 1.6 cm	28 g 0.9 cm
^{22}Na (cpm/dpm)	0.51 X 0.51		0.0111	0.0273	
	Σ 0.51 X 1.27		0.00247	0.0087	
	Σ 0.51 X 1.78		0.00231	0.0140	
^{26}Al (cpm/dpm)	0.51 X 0.51	0.0121	0.00941	0.0267	0.0293
	Σ 0.51 X 1.81	0.00228	0.00183	0.0072	0.0086
	Σ 0.51 X 2.32	0.00201	0.00133	0.0092	0.0129
$^{60}C_o$ (cpm/dpm)	Σ 1.17 X 1.33		0.00179	0.0088	
^{40}K (cpm/gK)	Σ 1.46	12.7	11.6	22.3	25.1
U (cpm/mgU)	Σ 0.61 X 0.77	0.377		1.17	
	Σ 0.61 X 1.12 to 1.24	0.781		2.77	
	Σ 0.61 X 1.38 to 1.51	0.191		0.75	
Th (cpm/mg Th)	Σ 0.28 X 2.61	0.133		0.283	
	Σ 0.58 X 2.61	0.163		0.508	
	Σ 0.86 X 2.61	0.027		0.104	

COUNTING RATE AND SPECIFIC ACTIVITY CALCULATIONS

Sample counting times varied from 4000 to about 10,000 minutes, depending primarily on mass and/or expected activity level. For coincident events where the sample counting rate is R_S and the total counts in the selected energy region G,

$$R_S = \frac{G}{T}, \text{ and } \sigma_S = \pm \ (G)^{1/2}/T$$

The net sample counting rate, R_N, is the difference between R_S and the background rate, R_B; $\sigma_N = \pm (\sigma_S^2 + \sigma_B^2)^{1/2}$. This net rate can be corrected, if necessary, for contributions from other nuclides. The corrected net counting rate is divided by the radionuclide counting yield ϵ_N and by the sample mass in kilograms to find the specific activity in disintegrations per minute per kilogram of sample (dpm/kg).

For ^{26}Al (in the absence of ^{22}Na), U, or Th, specific activities were calculated for three coincidence energy regions. The weighted average of the three calculated activity values was taken as the sample specific activity. Thus:

$$A = \frac{\sum\left(\frac{A_1}{\sigma_1^2} + \frac{A_2}{\sigma_2^2} + \frac{A_3}{\sigma_3^2}\right)}{\sum\left(\frac{1}{\sigma_1^2} + \frac{1}{\sigma_2^2} + \frac{1}{\sigma_3^2}\right)}$$

and

$$\sigma_A = \left[\frac{1}{\sum\left(\frac{1}{\sigma_1^2} + \frac{1}{\sigma_2^2} + \frac{1}{\sigma_3^2}\right)}\right]^{1/2}$$

The agreement in the pattern of counting rates for the three energy regions between sample and calibration source was checked by:

$$\chi_R^2 = \frac{\left(\frac{A - A_1}{\sigma_1}\right)^2 + \left(\frac{A - A_2}{\sigma_2}\right)^2 + \left(\frac{A - A_3}{\sigma_3}\right)^2}{2}$$

A value ≤ 1 indicates satisfactory agreement. If $\chi_R^2 > 1$, the calculated σ_A is multiplied by $\left(\chi_R^2\right)^{1/2}$ to provide a more realistic estimate of the activity uncertainty.

Where ^{22}Na and ^{26}Al were both present, constituting a mutual interference, the net counting rate data from the four coincidence energy regions (table 1) were treated as an overdetermined set of simultaneous linear equations. The four equations, of the form $Y \pm \sigma_Y = a_1 x_1 + a_2 x_2$, were reduced by least squares regression, weighted by $(\sigma_Y)^{-2}$. In this specific case, Y is the net counting rate, a_1 is the counting yield for one component (e.g., ^{22}Na) in a given energy region, x_1 is the concentration of that component, and a_2 and x_2 refer likewise to the second component (e.g., ^{26}Al).

Potassium was determined from the net 1.46-MeV peak extending above the combined non-coincident gamma-ray spectrum. Thus the counting rate, R_S, of the sample was obtained from the counts, C, in and on either side of the full energy peak:

$$R_S = \frac{C\,(\text{ch } 30\text{-}33) - C\,(28 + 29 + 34 + 35)}{T}$$

and

$$\sigma_S = \frac{[C\,(30\text{-}33) + C\,(28 + 29 + 34 + 35)]^{1/2}}{T}$$

The net K counting rate was found, as in the coincidence counting case, by $R_S - R_B$.

RESULTS

Measured specific activities, in dpm/kg at time of fall, for recently fallen chondrite samples studied in this laboratory are given in table 3. All U and Th values were calculated assuming that measured ^{208}Tl and ^{214}Bi were in radioactive equilibrium with their respective parents, ^{232}Th and ^{238}U. The Murchison sample was obtained from the University of Melbourne, Australia; the Havero sample consisted of numerous small fragments obtained from the University of Turku, Finland. Halflives of the cosmogenic radionuclides are given in each column. Data that have already been published are so cited in the reference column.

Measured specific activities of finds and old observed falls, the former identified by year only, are given in table 4. The Keyes samples are portions of cores obtained from D. Bogard of Johnson Space Center. The Pribram samples were obtained from Z. Ceplecha of the Ondrejov Observatory, Czechoslovakia, through R. McCrosky of the Smithsonian Astrophysical Observatory. The Wellington samples were provided by E. King, University of Houston. The Zerga amphoterite sample was provided by R. Fudali, Smithsonian Institute.

Table 5 contains radioactivities in achondrites measured in this laboratory. The Moama sample was provided by J. Lovering, University of Melbourne. The Norton County samples were obtained from K. Keil, University of New Mexico.

Table 3
Short-lived Radioactivities in Meteorites

Meteorite	Class	Recovered Mass - kg	Date of Fall	Sample ID	Sample Size - g	^{22}Na dpm/kg (2 6 y)	^{26}Al dpm/kg (740,000 y)	^{46}Sc dpm/kg (84 3 d)	^{48}V dpm/kg (16 d)	^{54}Mn dpm/kg (313 d)	^{60}Co dpm/kg (5 26 y)	K ppm	Ref
Barwell	L6	47	12/24/65	NMNH*	1265	84 0 ±4 0	51 0 ±4 0	9 0 ±3 0		85 0 ±5 0	6 0 ±1 0	1150 ±50	1
St Séverin	LL6	277	6/27/66	DIII$_1$	1293	102 0 ±3 0	55 0 ±5 0	5 0 ±1 0	16 0 ±5 0	64 0 ±6 0	1 9 ±0 7	790 ±20	1
				DIII$_2$ (2)	221		57 0 ±2 0						
Tathlith	L6	2	10/5/67	NMNH	192	85 0 ±3 0	59 0 ±3 0	4 4 ±1 2	19 0 ±12 0	59 0 ±6 0	2 8 ±0 5	740 ±30	1
Allende	C3	>2000	2/8/69	NMNH 3530	604	81 0 ±2 0	48 0 ±2 0	7 2 ±1 3	7 0 ±4 0	108 0 ±4 0	77 0 ±2 0	270 ±20	4
				3531	598	84 0 ±2 0	52 0 ±2 0	4 4 ±1 2	11 0 ±3 0	104 0 ±4 0	90 0 ±2 0	240 ±20	4
				3529a	124	89 0 ±4 0	52 0 ±3 0			118 0 ±14 0	181 0 ±5 0	230 ±20	4
				3529b	124	85 0 ±5 0	52 0 ±2 0			111 0 ±12 0	185 0 ±6 0	300 ±30	4
				3529c	200	89 0 ±3 0	62 5 ±2 2			126 0 ±11 0	166 0 ±4 0	300 ±30	4
Murchison	C2		9/28/69	#22	152	90 0 ±2 0	43 0 ±2 0	7 8 ±3 5		101 0 ±2 0	79 0 ±3 0	390 ±20	4
Lost City	H5	17	1/3/70	NMNH 4848	416	74 0 ±2 0	62 0 ±1 0	10 1 ±0 5	11 0 ±1 0	85 0 ±4 0	1 9 ±0 4	710 ±10	3
Ucera	H5	4 6	1/16/70	NMNH 5292	127	60 0 ±4 0	43 0 ±3 0	7 9 ±3 4		61 0 ±4 0	5 5 ±1 6	710 ±20	3
Malakal	L5	2	8/15/70	NMNH 5446	172	77 0 ±4 0	81 0 ±4 0	6 4 ±4 9		54 0 ±3 0	< 3 6	820 ±20	7
Dwaleni	H5	3 2	10/12/70	NMNH 5447	116	67 0 ±2 0	58 0 ±3 0	7 8 ±2 1	9 3 ±7 0	73 0 ±3 0	< 2 2	850 ±30	
Wethersfield	L5	0 4	4/8/71	NMNH 5596	284	56 7 ±2 3	48 7 ±3 6	6 9 ±1 6	10 2 ±4 0	48 0 ±5 0	< 2 3	820 ±10	
Havero	U	1 5	8/2/71		86	71 0 ±3 0	43 0 ±3 0	3 4 ±2 1		29 0 ±7 0	< 0 7	33 ±35	5
Gurbga	L5	0 3	2/26/72	NMNH 5675	220	70 9 ±4 7	55 6 ±4 1			64 9 ±7 4	3 2 ±2 8	785 ±21	
Canon City	H5	1 4	8/27/73	NMNH 5733	56	71 5 ±4 1	42 5 ±4 1	16 8 ±4 5		101 0 ±10 0	< 7 8	763 ±44	

*NMNH = National Museum of Natural History

Table 4
Radioactivities in Chondrites

Meteorite	Class	Recovered Mass - kg	Date of Fall/Find	Sample ID*	Sample Size - g	^{26}Al dpm/kg	K ppm	U ppb	Th ppb	Ref
Bath Furnace	L6	93	11/15/02	NMNH 302	322	53.0 ±4.0	600 ±30			†
Pierceville	L	2	1939	NMNH 1485	181	66.0 ±3 0	898 ±36			†
Lua	L5	9	6/26/26	ASU 613 1	40	70 6 ±4.1	964 ±85			6
Cannakkale	L	4	7/64	ASU 731	34	49.4 ±4.6	737 ±85			6
Narellan	L6	0.4	4/8/28	NMNH 1459	29	44.7 ±4.2	669 ±74			6
				Australia	33	49.4 ±4 6	881 ±85			6
Beenham	L5	44	1937	ASU 414.100a	269	62.0 ±1.5	840 ±10	58 ±9	45 ±24	†
Norcateur	L6	3	1940	ASU 525 30	72	52.1 ±3 4	1019 ±56	320 ±20		6
Finney	L5	10	1962	AML (2) 707.41	34	52 3 ±3.5	672 ±69	249 ±27	<152	6
Densmore	L6	11	1950	AML H41.47	202	64 3 ±3.8	466 ±18	30 ±8	55 ±28	
Wickenburg	L5	9	1940	ASU 449.8x	102	61.0 ±2.3	841 ±27	23 ±12	<126	
Armel	L5	9	1967	AML H71.27	80	58.9 ±2.7	657 ±40	38 ±14	104 ±61	
Kyle	L6	8	1965	AML H33.3	130	66.9 ±3.0	606 ±42	<23	70 ±36	
Keyes	L6	142	1939	JSC 3 H	21	68.9 ±5.4	834 ±126	<93	<513	8
				3 C	28	56.0 ±3.2	674 ±83	43 ±32	<114	8
				3 Dl	19	56.8 ±4.6	637 ±122	<70	<224	8
				2 D	28	50.9 ±3.7	697 ±91	47 ±34	<170	8
				2 A	36	62.9 ±3.4	721 ±76	<84	<192	8
				2 Bl	27	63.8 ±4.1	519 ±94	<109	<194	8

*NMNH = National Museum of Natural History
ASU = Arizona State University
AML = American Meteorite Laboratory
JSC = Johnson Space Center, NASA
†Cressy, P.J., and D D. Bogard, "On the Calculation of Cosmic-Ray Exposure Ages of Stone Meteorites," *Geochim. Cosmochim. Acta*, 1976, in press.

Table 4 (Continued)

Meteorite	Class	Recovered Mass - kg	Date of Fall/Find	Sample ID*	Sample Size - g	^{26}Al dpm/kg	K ppm	U ppb	Th ppb	Ref
Shelburne	L5	19	8/13/04	ME 2142	98	79.4 ±2.0	780 ±30			
Claytonville	L	11	1964	AML 51.15	147	51.9 ±2.7	835 ±51	24 ±13	81 ±43	
Roy	L5	47	1933	AML 234.143	63	67.0 ±3.0	623 ±54	<46	<190	
Etter	L	46	1965	AML 47.3	276	42.2 ±1.2	538 ±14	24 ±6	30 ±23	†
Bowesmont	L6	2 3	1962	AML H6.21	29	59.1 ±3.4	788 ±90	68 ±25	<280	
Slobodka	L4	2.7	1818	ASU 730	25	60.3 ±4.9	970 ±160	<180	<240	
Atwood	L6	2	1949	AML H4.22	20	68.2 ±6.2	883 ±130	158 ±44	<427	
Callihan	L6	40	1958	AML 670 98	55	68.0 ±3.1	709 ±55	32 ±18	<136	
Fremont Butte	L4	7	1963	AML H5 27	35	72.9 ±4.0	586 ±85	79 ±28	<246	
Kinley	L	2	1965	AML H88.5	62	69.2 ±3.1	721 ±53	<46	<186	
Grassland	L4		1964	AML H23 8	11	71.5 ±8.0	660 ±250	313 ±72		
Dalgety Downs	L4, 5	432	1941	AMNH 4190 A	151	46.5 ±1.9	1066 ±64	630 ±80	260 ±40	†
				E	49	49 4 ±2.8	980 ±100	207 ±25	<185	†
				D	122	40.3 ±2.6	939 ±63	222 ±18	112 ±55	†
				F	99	49.9 ±2.1	869 ±64	235 ±21	<220	†
Plainview	H5	700	1917	AML (2) 92.26	284	59.0 ±2.0				
Dimmit	H3, 4	14	1947	AML H9.50	413	44 0 ±2.0	730 ±10			
Ehole	H5	2 4	8/31/61	NMNH 2142	1472	49.0 ±3.0				2

*ME = Field Museum of Natural History, Chicago
AML = American Meteorite Laboratory
ASU = Arizona State University
AMNH = American Museum of Natural History
NMNH = National Museum of Natural History
†Herzog, G.F. and P.J. Cressy, "^{26}Al Losses from Weathered Chondrites," *Meteoritics*, 1976, in press.

Table 4 (Continued)

Meteorite	Class	Recovered Mass - kg	Date of Fall/Find	Sample ID*	Sample Size - g	^{26}Al dpm/kg	K ppm	U ppb	Th ppb	Ref
Pribram	H5	9 5	4/7/59	C_3 #680	104	59 0 ±3.0	610 ±40			
				C_3 #393	428	52.0 ±2 0	750 ±20			
					4270	52.0 ±6.0				
Bur-Gheluai	H5	120	10/16/19	NMNH 778	184	30 2 ±1.8	770 ±40			†
Sena	H4	4	11/17/1773	NMNH 1473	148	33.3 ±2.0	1010 ±50			†
Morland	H6	285	1890	NMNH 934	294	40.5 ±2 0	726 ±22			†
Cavour	H6	24	1943	NMNH 1411	334	60.0 ±2.0	680 ±20			†
Wellington (a)	H	13	1955	E. KING	69	56.5 ±2.1	580 ±30			6
Wellington (b)				E. KING	41	60.3 ±6.3	543 ±67	46 ±25		6
Ozona	H	128	1929	ME 2335	103	65.0 ±2 5	573 ±33			6
Pokhra	H5	0.4	5/27/1866	CAL 149	14	39.7 ±5.5	620 ±140			6
Gopalpur	H	1.6	5/23/1865	CAL 175	13	29.9 ±6.4	740 ±150			6
Cee Vee	H5	3 6	1959	AML H25 16	88	63.1 ±2 4	651 ±31	38 ±12	127 ±43	
Wellman	H5	50	1940	AML H12.55	162	72.4 ±2 4	575 ±21	12 ±9	<130	6
Clovis #2, a	H6	34	1960	AML H8 19	80	75.4 ±2.6	641 ±40	31 ±14	72 ±49	
Clovis #2, b				AML H8 66	102	70.2 ±2.0	735 ±44	64 ±12	<80	
Menow	H4	11	10/7/1862	ME 1388	24	53 7 ±5 8	794 ±127			
Bath	H4	21	8/29/1892	ME 1782	93	66.0 ±2.4	775 ±34			

*NMNH = National Museum of Natural History
ME = Field Museum of Natural History, Chicago
AML = American Meteorite Laboratory
CAL = Calcutta, India

†Cressy, P.J., and D D Bogard, "On the Calculation of Cosmic-ray Exposure Ages of Stone Meteorites," *Geochim. Cosmochim. Acta*, 1976, in press.

Table 4(Continued)

Meteorite	Class	Recovered Mass - kg	Date of Fall/Find	Sample ID*	Sample Size - g	^{26}Al dpm/kg	K ppm	U ppb	Th ppb	Ref
Bledsoe	H	31	1970	AML H121.36	109	44.8 ±2.0	386 ±36	32 ±14	76 ±44	†
Tieschitz	H3/C3	28	7/15/1878	ME 1726	21	78.0 ±7.0	160 ±160			6
Felt				AML H114.9	93	65.5 ±3.8	610 ±35	39 ±13	<78	
Leoville	C3	8	1961	AML H40.72	62	60.1 ±2.7	151 ±45	52 ±16	<209	
Seminole #2		1	1965	AML H43.3	88	48.9 ±3.1	589 ±64	217 ±25	<160	†
Seminole #3		1.7	1967	AML H73.4	15	64.6 ±6.0	663 ±171	175 ±60		
Zerga	LL6	0.1	1973	NMNH 5740	74	51.5 ±3.4	1018 ±60	186 ±28	<170	§

*AML = American Meteorite Laboratory
ME = Field Museum of Natural History, Chicago
NMNH = National Museum of Natural History

†Herzog, G.F., and P.J. Cressy, "^{26}Al Losses from Weathered Chondrites," *Meteoritics*, 1976, in press.

§Fudali, R F., and P J. Cressy, "Investigation of a New Stony Meteorite from Mauritania with Some Additional Data on Its Find Site Aouelloul Crater," *Earth and Planetary Science Letters*, 1976, in press.

ORDINARY CHONDRITES

Chondrite chemical analyses typically show K = 700 to 900 ppm and U on the order of 20 ppb. A number of the weathered meteorite finds in table 4 have significantly lower K content (see figure 3) and/or higher U (or its daughters). These alterations can be attributed to the weathering process itself, sometimes leaching K from the meteorite and sometimes introducing U (and Th) or their decay products into the sample. Although these weathering effects do not always correspond to diminished ^{26}Al activities in table 4, the converse is true; significantly reduced ^{26}Al levels (not attributable to cosmic-ray shielding or short exposure age) are invariably associated with low K and/or high U contents. Specifically:

Etter	^{26}Al = 42.2 dpm/kg	K = 538 ppm, but U = 24 ppb
Dalgety Downs	^{26}Al = 40.3 to 49.9 dpm/kg	U = 207 to 630 ppm, but K = 869 to 1066 ppb
Bledsoe	^{26}Al = 44.8 dpm/kg	K = 386 ppm, but U = 32 ppb
Seminole #2	^{26}Al = 48.9 dpm/kg	K = 589 ppm, but U = 217 ppb

Expected ^{26}Al activities under average cosmic-ray shielding conditions can be calculated from chemical compositions using target element production rates (Reference 2). This average production rate does not take into account the effects of sample depth and meteorite preatmospheric size (References 6 and 8). The spallation ^{22}Ne/^{21}Ne ratio has been shown to be an indicator of irradiation hardness (Reference 10), and thus (References 6, 8, 11, and 12) related to shielding (size and depth).* In figure 4, the ratio of measured ^{26}Al to that calculated from chemical composition (^{26}Al)/(^{26}Al$_0$) is plotted against ^{22}Ne/^{21}Ne for meteorites in which both measurements were made on the same sample. The upper line represents the trend reported by Herzog and Cressy (Reference 6) for data obtained from a number of chondrites. The lower line was calculated from the data (♦) obtained on core samples of the Keyes chondrite (References 8 and 11). The first relationship reflects a variety of unknown sizes and depths, while the latter is due only to depth variations in a single fairly large stone meteorite.

The difference in slope between the two lines, and the tendency of the data to scatter around them, suggests that the ^{22}Ne/^{21}Ne ratio is not entirely adequate as an indicator of both size and depth effects on ^{26}Al production (Reference 6). The Herzog-Cressy line is most likely an approximation to a family of curves, similar to the Keyes line (although not necessarily linear) but with slopes dependent on meteorite preatmospheric size.

The Dalgety Downs data (○) fall conspicuously below the trend of the other data in the diagram, probably because of terrestrial weathering.† The St. Séverin (SS) data point

*Cressy, P.J. and D.D. Bogard, "On the Calculation of Cosmic-Ray Exposure Ages of Stone Meteorites," *Geochim. Cosmochim. Acta*, 1976, in press.

†Herzog, G.F. and P.J. Cressy, "^{26}Al Losses from Weathered Chondrites," *Meteoritics*, 1976, in press.

Table 5
Radioactivities in Achondrites

Meteorite	Class	Recovered Mass - kg	Date of Fall/Find	Sample ID*	Sample Size - g	^{26}Al dpm/kg	K ppm	U ppb	Th ppb	Ref
Kenna	U	10.9	1972	AML H159.3	42	49.3 ±3.7	92 ±68	<84	<174	†
Moama	Eu	3.4	1940	Melbourne	61	86.5 ±3.5	47 ±57	<55	<191	
Nuevo Laredo	Eu	0.5	1950	NMNH 1783	132	81 5 ±2.1	355 ±38	109 ±22	385 ±57	
Cachari	Eu	23 5	1921	NMNH 5309	203	69.8 ±2.2	402 ±26	196 ±22	376 ±59	
Yurtuk	Ho	1	4/2/36	NMNH 1422	31	71.1 ±4.7	<340	134 ±38	185 ±124	
Bununu	Ho	0.4	fell 1942	NMNH 1571	77	99.1 ±3.4	214 ±47	55 ±20	189 ±75	
Binda	Ho	5.5	1912	NMNH 1757	72	97.4 ±3.1	72 ±49	<53	81 ±75	
Shallowater	Au	4.7	1936	ASU 318 9	135	62.8 ±2.0	230 ±22	50 ±9	86 ±30	§
Bustee	Au	2	2/12/1852	NMNH 5622	82	75.9 ±3 3	205 ±47	<30	<160	§
Khor Temiki	Au	3	4/8/32	NMNH 1551	83	89 9 ±3.5	432 ±77	<40		§
Pesyanoe	Au	3	10/2/33	NMNH 1425	66	98.4 ±3.4	584 ±57			§
Norton	Au	>1100	2/18/48	N23-5 (NM)	214	97.6 ±3.3	210 ±30		<60	§
County				N102	456	79.0 ±2.7	<30	<15	<46	§
Garland	D	0 1	~1955	NMNH 2140	94	84.1 ±3.8	<150	<58	<180	‡
Tatahouine	D	12	7/27/31	ME 2651	83	79.4 ±3.3	<60	<19	<58	‡

*AMU = American Meteorite Laboratory
NMNH = National Museum of Natural History
ASU = Arizona State University
ME = Field Museum of Natural History, Chicago

†Cressy, P J., "^{26}Al in Kenna and Other Ureilites," *Geochim. Cosmochim. Acta*, 1976, in press.

§Herzog, G.F. and P.J. Cressy, "The Cosmic-Ray Exposure of Aubrites," 1976, in preparation.

‡Herzog, G.F. and P.J. Cressy, "Diogenite Exposure Ages," *Geochim. Cosmochim. Acta*, 1976, in press.

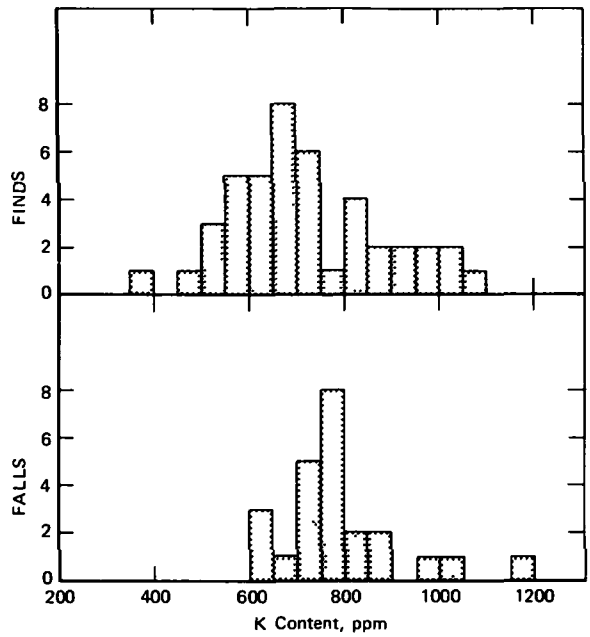

Figure 3. The distribution of measured potassium contents (tables 3 and 4) for H, L, and LL chondrite finds and observed falls.

(Reference 13) was obtained from a very near surface sample; other data from this meteorite fall much nearer the Herzog-Cressy line. Ucera (U) appears to have experienced a two-stage irradiation (Reference 14). The $^{22}Ne/^{21}Ne$ ratio primarily reflects shielding conditions during the first, relatively long irradiation, while the ^{26}Al activity was produced during the last few million years, after Ucera had been reduced to a smaller body by an intervening collision.

Five meteorites lie considerably above the field of data. Malakal experienced a uniquely high cosmic-ray exposure (Reference 7). The same explanation may apply to Shelburne (S), Clovis #2 (C), Kabo (K), and Tieschitz (T) as well (Reference 6). Appley Bridge, Cavour, and Morland were not plotted because noble gas data indicate short cosmic-ray exposure ages and thus ^{26}Al undersaturation.* However, their ^{26}Al activities are inconsistently large for the estimated ages and may be best explained by an increased cosmic-ray flux also.

FRESHLY-FALLEN METEORITES

Although the relationship of ^{26}Al production to the neon isotope ratio is not as tight as one would like, the empirical relationship calculated by Herzog and Cressy (Reference 6) does provide an improved basis for estimating ^{21}Al production rates in individual meteorite samples.

*Cressy, P.J. and D.D. Bogard, "On the Calculation of Cosmic-Ray Exposure Ages of Stone Meteorites," *Geochim. Cosmochim. Acta*, 1976, in press.

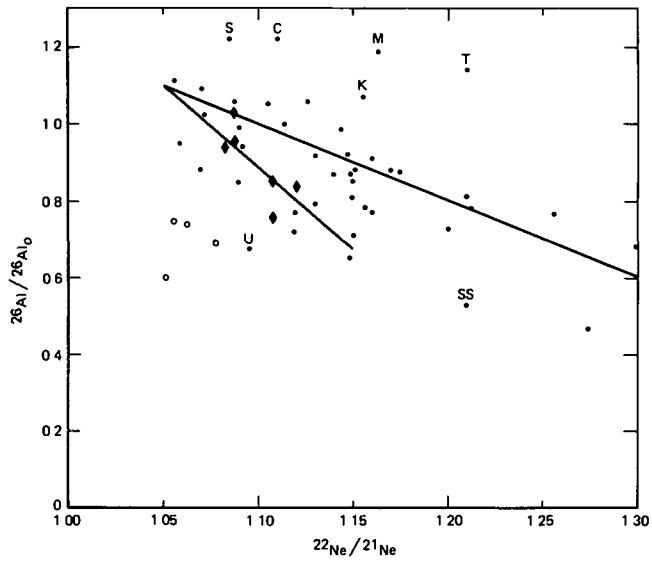

Figure 4. The ratio of observed to calculated ^{26}Al activity plotted against spallation $^{22}Ne/^{21}Ne$ ratio in H, L, and LL chondrites. Diamonds (♦) are core data from the Keyes chondrite (References 8 and 11). Open circles (○) are data for Dalgety Downs.* Symbols are identified in the text. The equation for the upper line (Reference 6) is: $^{26}Al/^{26}Al_0 = 3.2 - 2.0\ (^{22}Ne/^{21}Ne)$. The lower line is taken from the Keyes data: $^{26}Al/^{26}Al_0 = 5.55 - 4.24\ (^{22}Ne/^{21}Ne)$. The data are taken from tables 3 and 4 and from the literature (References 6, 9 through 18, and others).†

Unfortunately, not nearly as much data exist on short-lived radionuclides as on long-lived ^{26}Al, due to the rarity of meteorite falls. The data in table 3 probably represent more than one-fourth of all such data measured to date in meteorites shortly after their fall. With such a paucity of data, it is difficult to search for trends. Data for meteorites in which ^{22}Na, ^{46}Sc, ^{54}Mn, and noble gases were measured in the same sample are plotted in figure 5.

No clear correlations are apparent. Larger specific activities of these nuclides have been reported in some meteorites, but are not plotted because no corresponding neon isotope data exist. An additional complicating factor exists because of the relatively short half-lives of these nuclides. Their time-of-fall specific activities are potentially sensitive to spatial variations in cosmic-ray flux density and may be significantly affected by exposure to solar flare activity.

*Herzog, G.F. and P.J. Cressy, "^{26}Al Losses from Weathered Chondrites," *Meteoritics*, 1976, in press.

†Cressy, P.J. and D.D. Bogard, "On the Calculation of Cosmic-ray Exposure Ages of Stone Meteorites," *Geochim. Cosmochim. Acta*, 1976, in press.

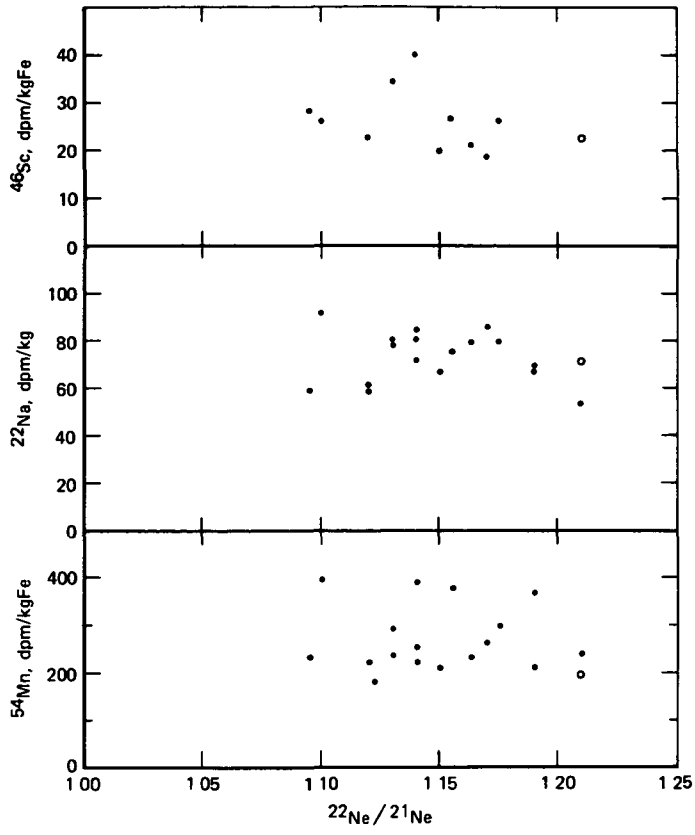

Figure 5. ^{46}Sc and ^{54}Mn, normalized to target element composition, and ^{22}Na, plotted against ^{22}Ne/^{21}Ne ratio. The open circle (o) represents the Haverö ureilite; its ^{22}Ne/^{21}Ne ratio has been normalized to chondrite chemistry using the Mg/Si weight ratio.*

Figure 6 is a plot of ^{22}Na against ^{26}Al. A general positive correlation is apparent; note the Malakal point with its conspicuously high ^{26}Al activity. In figure 7, ^{46}Sc is also positively correlated with ^{54}Mn, although standard deviations of ^{46}Sc activities are typically about 20 percent. The correlation is somewhat surprising in this case, because ^{46}Sc is a relatively high-energy product of cosmic-ray interactions with iron, while ^{54}Mn is definitely a low-energy product.

^{26}Al IN ACHONDRITES

Achondrite isotope data can not be compared directly with chondrite data because of the considerable differences in chemical composition. The ratio of ^{26}Al against $^{26}Al_0$, the production rate calculated from target element chemistry (Reference 2), will in principle

*Cressy, P.J. and D.D. Bogard, "On the Calculation of Cosmic-ray Exposure Ages of Stone Meteorites," *Geochim. Cosmochim. Acta*, 1976, in press.

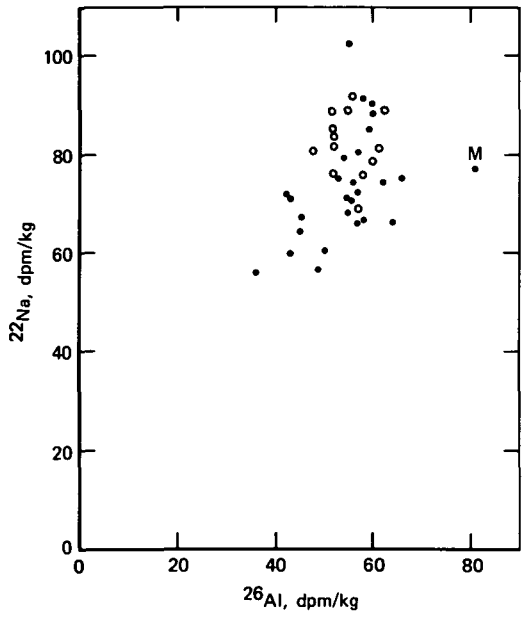

Figure 6. Variation of ^{22}Na with ^{26}Al activity. The open circles (○) are data for Allende (Reference 4). The anomalous Malakal data point is identified by M.

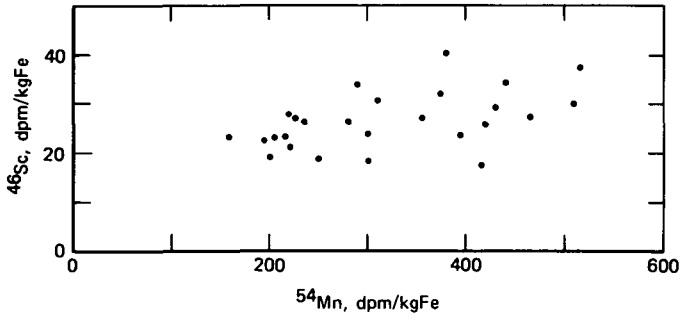

Figure 7. Variation of ^{46}Sc with ^{54}Mn, in dpm per kilogram of the principal target element for nuclear production.

account for this effect; however, for extremely different chemistries, as in eucrites and howardites, the corrections are less certain. Cressy and Bogard* empirically determined an equation to adjust ^{22}Ne/^{21}Ne ratios for chemistry differences:

$$(F_{22/21})_{chem} = 1.122 - 0.224 \frac{[Mg]}{[Si]} + 0.09 \frac{[Mg]^2}{[Si]^2}$$

*Cressy, P.J. and D.D. Bogard, "On the Calculation of Cosmic-ray Exposure Ages of Stone Meteorites," *Geochim. Cosmochim. Acta*, 1976, in press.

Dividing measured neon isotope ratios by $(F_{22/21})_{chem}$ yields the chondrite chemistry equivalent of the observed ratios. Thus, plots of $^{26}Al/^{26}Al_0$ against the adjusted $^{22}Ne/^{21}Ne$ ratio can be compared with the corresponding plot for ordinary chondrites (figure 4).

Figure 8 is such a plot for howardites, eucrites, and the Nakhla achondrite (included here because it is a single-meteorite class whose chemical composition most closely resembles the calcium-rich achondrites). Several features are apparent from this plot.

- Eucrite and howardite data seem to be randomly intermingled, although their Mg, Ca, and Al contents are significantly different. The ^{26}Al production rates ($^{26}Al_0$) calculated (Reference 2) from average eucrite and howardite chemical compositions are 136 and 112 dpm/kg, respectively. The difference is due primarily to the production rate from Al ($P_{26}Al$). An error in this rate would produce distinctly different values of $^{26}Al/^{26}Al_0$ for the two classes; the pattern of eucrite and howardite data in figure 8 supports $P_{26}Al = 113$ dpm/kg Al (Reference 2).

- Yet, for the most part, the Eu and Ho ^{26}Al data fall appreciably beneath not only the Herzog-Cressy chondrite trend, but the Keyes depth correlation as well. On the other hand, Nakhla, with a lower, almost chondritic, Al content, lies much nearer the chondrite data. An overestimated $P_{26}Al$ could yield the kind of discrepancy observed between Nakhla and the aluminum-rich achondrites. As noted above however, this would also have resulted in the segregation of eucrites and howardites from each other.

  Another possible explanation was suggested several years ago (Reference 2) on the basis of less information. It is conceivable that eucrites and howardites as a group may have been exposed to a lower cosmic-ray flux than that experienced by most chondrites. This would require an unknown but exotic orbit for essentially two entire classes (perhaps related) of meteorites, despite whatever collisions they may have undergone in their individual histories.

- None of the samples in figure 8 have adjusted $^{22}Ne/^{21}Ne$ ratios greater than 1.14; some are as low as 1.03. The raw data for these samples lie between 1.10 and 1.22, slightly above a typical chondrite range. This pattern could be due at least in part to the Mg/Si normalization. The Bruderheim data used for the normalizing equation* did not include samples having such low Mg/Si ratios. Data from Elenovka olivine (Reference 19), Mg/Si <0.2, was used to fix the curve at the low-Mg end. It is possible the equations could have "overadjusted" the $^{22}Ne/^{21}Ne$ ratios for these meteorites (Mg/Si = 0.2 to 0.4), but not by more than about 0.02 units.

*Cressy, P.J. and D.D. Bogard, "On the Calculation of Cosmic-ray Exposure Ages of Stone Meteorites," *Geochim. Cosmochim. Acta*, 1976, in press.

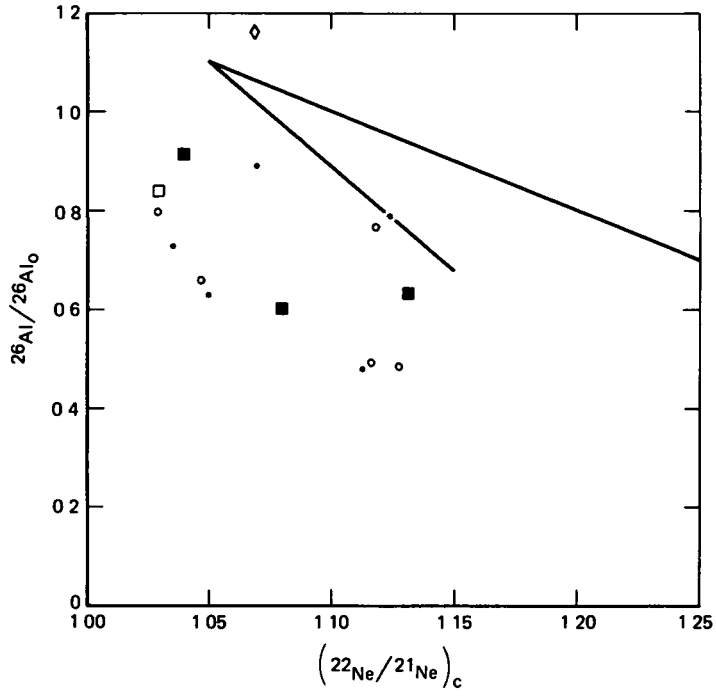

Figure 8. Ratio of observed to calculated ^{26}Al activities in eucrites (○), howardites (■), and Nakhla (◊), plotted against $^{22}Ne/^{21}Ne$ ratios adjusted to chondrite-chemistry equivalents (see text). Solid points represent ^{26}Al and neon data obtained on the same sample. The trend lines are those described in figure 4. The chemistry adjustments to $^{22}Ne/^{21}Ne$ lowered this ratio about 0.07 eucrites and 0.05 for howardites.

Another possibility is that eucrites and howardites are typically much larger than most chondrites. It has been shown by a number of investigators that $^{22}Ne/^{21}Ne$ ratios decrease with increasing size and/or depth, due to the increasing proportion of low-energy secondary cosmic rays produced within the meteorite. In principle, sufficiently large size/depth should result in decreased ^{26}Al production also. This has not been unambiguously observed experimentally, due presumably to the rarity of such large chondrites. All in all, this possibility does not seem too likely.

A third possibility is exposure to an unusually soft cosmic-ray spectrum; that is, a high proportion of low-energy radiation. This alternative would again require unique orbits for these meteorites. The most likely region would be relatively near the sun, where the large flux of low-energy solar protons and enhanced solar modulation of galactic cosmic rays could yield the observed low values of $^{22}Ne/^{21}Ne$ and $^{26}Al/^{26}Al_0$. The frequently-observed ^{3}He loss for these meteorites could then be explained by solar heating. It must be noted that this speculation benefits from our poor knowledge of other regions of the solar system.

The aubrite data in figure 9 roughly parallel the chondrite trend, but with higher ^{26}Al ratios.* Although the discrepancies are not great, they form a consistent trend. If real, this trend suggests an intriguing possibility. The Malakal chondrite was shown to have experienced an uniquely high cosmic-ray flux (Reference 7). If aubrites were exposed to a similar but less extreme flux, their ^{26}Al activities would be consistent with the data in figure 9. There is some circumstantial evidence for this "unique orbit" alternative.

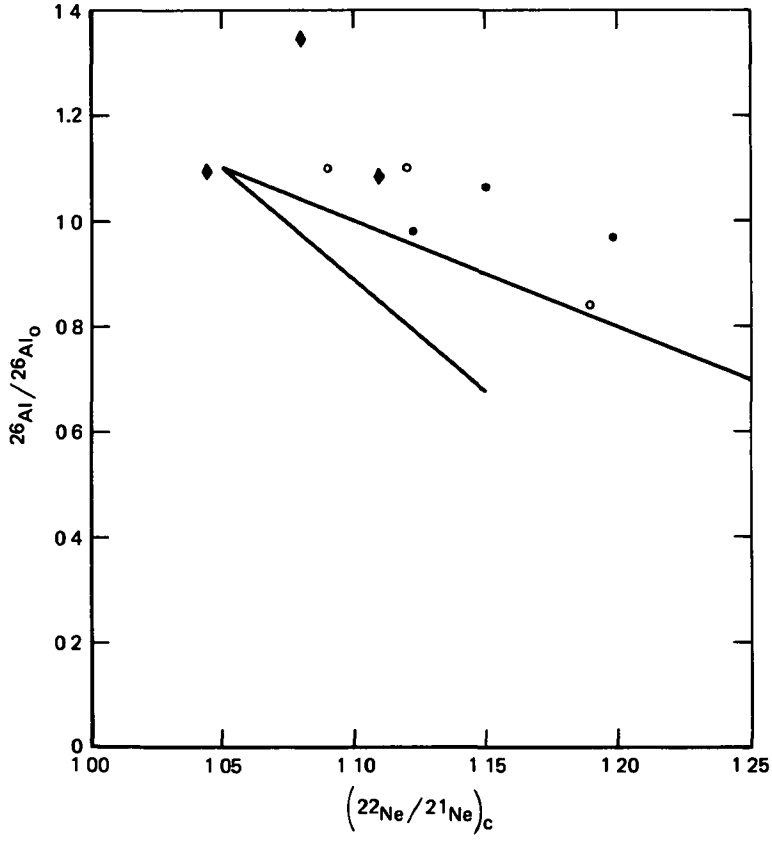

Figure 9. Variation of $^{26}Al/^{26}Al$ in aubrites with the $^{22}Ne/^{21}Ne$ ratio. The diamonds (♦) are Norton County data (Reference 20).* As before, solid points represent same sample measurements. No chemistry adjustment to $^{22}Ne/^{21}Ne$ was required.

Aubrite cosmic-ray exposure ages are typically greater than 30×10^6 years; the mean for 9 aubrites is 36 with a range of 8 (Aubres) to 76 (Norton County). Bishopville, Bustee, Cumberland Falls, and Khor Temiki have apparent ages between 36 and 40 million years, and may represent products of a single collision. The mean collisional lifetime for aubrites is appreciably longer than that of any other stone meteorite class. Either aubrites are much

*Herzog, G.F. and P.J. Cressy, "The Cosmic-ray Exposure of Aubrites," 1976, in preparation.

"tougher" than other stones (demonstrably not the case), or they traverse orbits in which the probability of encountering other objects is much less than for chondrites. This hypothesis is worthy of further study.

The existing diogenite data are shown in figure 10 and have been discussed in some detail by Herzog and Cressy.* The data generally lie near the chondrite trend, although Garland may have an anomalously high ^{26}Al activity. The noble gas data clearly imply* that eight of the nine known diogenites are products of just two collisions that occurred 14 and 23 million years ago, respectively.

The ureilite data (figure 11) are discussed in more detail elsewhere.† Recovered masses are typically small, and $^{22}Ne/^{21}Ne$ ratios rather high, suggesting that the preatmospheric masses of ureilites are also generally small. With the exception of Dyalpur, the data cluster very well along the chondrite trend. The pattern is convincing. The earlier suggestion of a unique orbit and a low cosmic-ray flux to explain low ureilite ^{26}Al activities (References 5 and 21) is clearly unnecessary.†

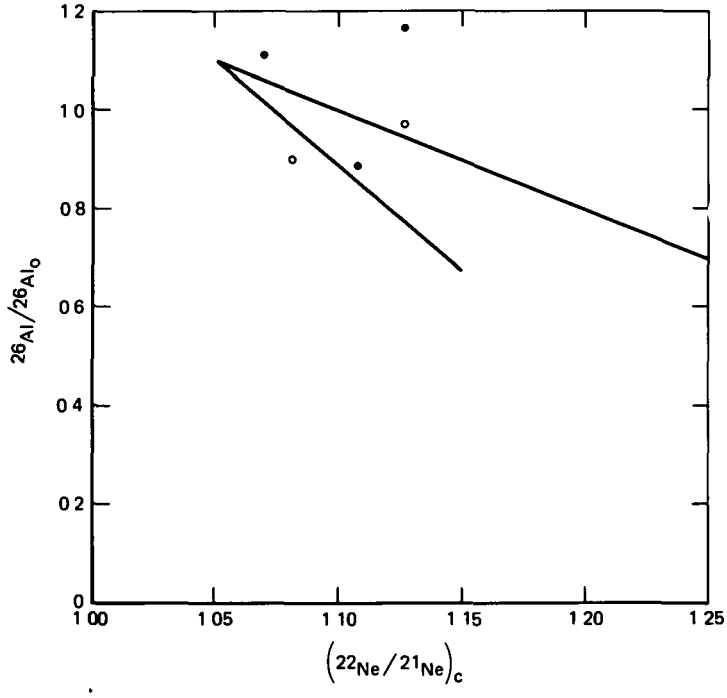

Figure 10. $^{26}Al/^{26}Al_0$ in diogenites against adjusted $^{22}Ne/^{21}Ne$. Solid points are same sample measurements. The $^{22}Ne/^{21}Ne$ adjustment lowered measured values about 0.02 units.

*Herzog, G.F. and P.J. Cressy, "Diogenite Exposure Ages," *Geochim. Cosmochim. Acta*, 1976, in press.

†Cressy, P.J., "^{26}Al in Kenna and Other Ureilites," *Geochim. Cosmochim. Acta*, 1976, in press.

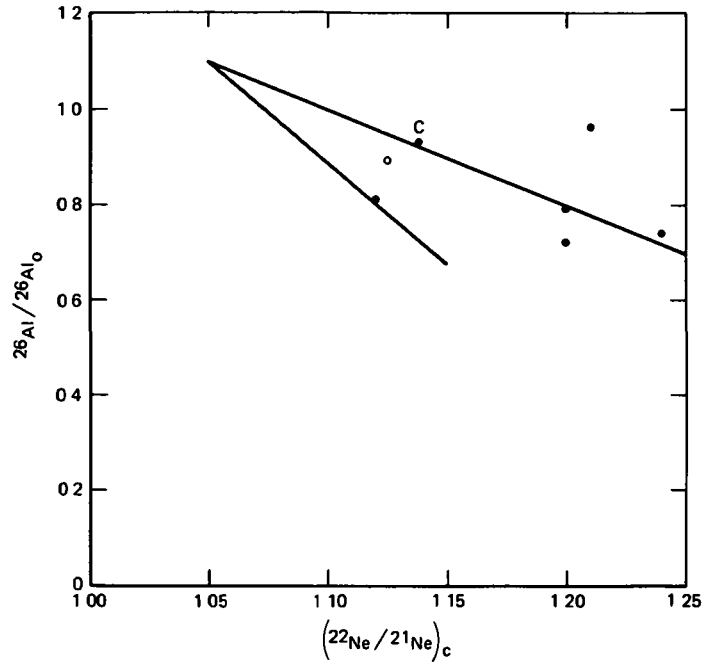

Figure 11. $^{26}Al/^{26}Al_0$ in ureilites and Chassigny (c) against adjusted $^{22}Ne/^{21}Ne$. Chassigny is a single meteorite class whose chemical composition most closely resembles those of ureilites. Kenna (○) is the only ureilite for which the same sample criterion is not known to apply. Chemistry normalization raised $^{22}Ne/^{21}Ne$ about 0.02 units.

Goddard Space Flight Center
National Aeronautics and Space Administration
Greenbelt, Maryland April 6, 1976

REFERENCES

1. Cressy, P.J., "Multiparameter Analysis of Gamma Radiation from the Barwell, St. Séverin and Tatlith Meteorites," *Geochim. Cosmochim. Acta*, **34**, 1970, pp. 771-779.

2. Cressy, P.J., "The Production Rate of Al^{26} From Target Elements in the Bruderheim Chondrite," *Geochim. Cosmochim. Acta*, **35**, 1971, pp. 1283-1296.

3. Cressy, P.J., "Cosmogenic Radionuclides in the Lost City and Ucera Meteorites," *J. Geophys. Res.*, **76**, 1971, pp. 4072-4075.

4. Cressy, P.J., "Cosmogenic Radionuclides in the Allende and Murchison Carbonaceous Chondrites," *J. Geophys. Res.*, **77**, 1972, pp. 4905-4911.

5. Cressy, P.J., "Cosmogenic Radionuclides in the Havero Meteorite," *Meteoritics*, **7**, 1972, pp. 533-536.

6. Herzog, G.F. and P.J. Cressy, "Variability of the Al^{26} Production Rate in Ordinary Chondrites," *Geochim. Cosmochim. Acta*, **38**, 1974, pp. 1827-1841.

7. Cressy, P.J. and L.A. Rancitelli, "The Unique Cosmic-ray History of the Malakal Chondrite," *Earth Planet. Sci. Lett.*, **22**, 1974, pp. 275-283.

8. Cressy, P.J., "^{26}Al in Cores of the Keyes Chondrite," *J. Geophys. Res.*, **80**, 1975, pp. 1551-1554.

9. Fuse, K. and E. Anders, "Aluminum-26 in Meteorites–VI. Achondrites," *Geochim. Cosmochim. Acta*, **33**, 1969, pp. 653-670.

10. Eberhardt, P., O. Eugster, J. Geiss, and K. Marti, "Rare Gas Measurements in 30 Stone Meteorites," *Z. Naturforsch.*, **21a**, 1966, pp. 414-426.

11. Wright, R.J., L.A. Simms, M.A. Reynolds, and D.D. Bogard, "Depth Variation of Cosmogenic Noble Gases in the ~120-kg Keyes Chondrite," *J. Geophys. Res.*, **78**, 1973, pp. 1308-1318.

12. Schultz, L., D. Phinney, and P. Signer, "Depth Dependence of Spallogenic Noble Gases in the St. Séverin Chondrite," *Meteoritics*, **8**, 1973, pp. 435-436, Abstract.

13. Marti, K., J.P. Shedlovsky, R. Lindstrom, J.R. Arnold, and N. Bhandari, "Cosmic Ray Produced Radionuclides and Rare Gases Near the Surface of the St. Séverin Meteorite," In *Meteorite Research* (editor P.M. Millman), Reidel, 1969, pp. 246-266.

14. Bogard, D.D., R.S. Clark, J.E. Keith, and M.A. Reynolds, "Noble Gases and Radionuclides in Lost City and Other Recently Fallen Meteorites," *J. Geophys. Res.*, **76**, 1971, pp. 4076-4083.

15. Bogard, D.D., M.A. Reynolds, and L.A. Simms, "Noble Gas Concentrations and Cosmic Ray Exposure Ages of Eight Recently Fallen Chondrites," *Geochim. Cosmochim. Acta*, **37**, 1973, pp. 2417-2433.

16. Ganapathy, R. and E. Anders, "Noble Gases in Eleven H-chondrites," *Geochim. Cosmochim. Acta*, **37**, 1973, pp. 359-362.

17. Heymann, D. and E. Anders, "Meteorites with Short Cosmic Ray Exposure Ages as Determined from Their Al^{26} Content," *Geochim. Cosmochim. Acta*, **31**, 1967, pp. 1793-1809.

18. Nyquist, L., H. Funk, L. Schultz, and P. Signer, "He, Ne and Ar in Chondritic Ni-Fe as Irradiation Hardness Sensors," *Geochim. Cosmochim. Acta*, **37**, 1973, pp. 1655-1685.

19. Bochsler, P., P. Eberhardt, J. Geiss, and N. Grögler, "Rare-gas Measurements in Separate Mineral Phases of the Otis and Elenovka Chondrites," *Meteorite Research* (editor P.M. Millman) Reidel, pp. 857-874.

20. Herzog, G.F. and E. Anders, "Radiation Age of the Norton County Meteorite," *Geochim. Cosmochim. Acta*, **35**, 1971, pp. 239-244.

21. Wilkening, L.L., G.F. Herman, and E. Anders,"Aluminum-26 in Meteorites–VII. Ureilites, Their Unique Radiation History," *Geochim. Cosmochim. Acta*, **37**, 1973, pp. 1803-1810.

NASA-Langley, 1976

"The aeronautical and space activities of the United States shall be conducted so as to contribute . to the expansion of human knowledge of phenomena in the atmosphere and space. The Administration shall provide for the widest practicable and appropriate dissemination of information concerning its activities and the results thereof"

—NATIONAL AERONAUTICS AND SPACE ACT OF 1958

NASA SCIENTIFIC AND TECHNICAL PUBLICATIONS

TECHNICAL REPORTS Scientific and technical information considered important, complete, and a lasting contribution to existing knowledge

TECHNICAL NOTES Information less broad in scope but nevertheless of importance as a contribution to existing knowledge.

TECHNICAL MEMORANDUMS· Information receiving limited distribution because of preliminary data, security classification, or other reasons. Also includes conference proceedings with either limited or unlimited distribution.

CONTRACTOR REPORTS Scientific and technical information generated under a NASA contract or grant and considered an important contribution to existing knowledge

TECHNICAL TRANSLATIONS Information published in a foreign language considered to merit NASA distribution in English

SPECIAL PUBLICATIONS Information derived from or of value to NASA activities Publications include final reports of major projects, monographs, data compilations, handbooks, sourcebooks, and special bibliographies

TECHNOLOGY UTILIZATION PUBLICATIONS Information on technology used by NASA that may be of particular interest in commercial and other non-aerospace applications Publications include Tech Briefs, Technology Utilization Reports and Technology Surveys

Details on the availability of these publications may be obtained from:

SCIENTIFIC AND TECHNICAL INFORMATION OFFICE

NATIONAL AERONAUTICS AND SPACE ADMINISTRATION

Washington, D.C. 20546